The Effective Elastic Coefficients of Porous Media with Simple Pore Geometries - 14239

CHEO. K. LEE
Handong Global University
3 Namsong-ri, Heunghae-eub, Buk-gu, Pohang, Kyungbuk, 791-708
Republic of Korea

ABSTRACT

The effective macroscale elastic coefficients for porous media saturated by a liquid are calculated by numerically solving the micro-cell elastostatic problem defined in the process of applying the homogenization theory to periodic porous media. Two different types of pore geometry are considered: circular and rectangular. By minimizing a variational principle which is approximated by finite elements, the solid displacements in the solid region are obtained and are used to determine the effective elastic coefficients on the macroscale. Two groups of elastic coefficients are investigated: the conventional effective elastic coefficients caused by imposed macroscale strain and the pressure coefficients which signify the elastic response of the medium to the pore pressure change. It is shown that the elastic coefficients generally decrease whereas the pressure coefficients increase as the pore fraction increases.

INTRODUCTION

The elastic properties of subsurface geological formations are important physical characteristics for proper management of the underground repository. Alteration of stress field caused by various disturbances such as surcharge or overburden, pore pressure change, and temperature variation may impose some threat to the functioning of the underground facility. Therefore it is essential to know the elastic characteristics of the underground rock medium which in general has pores of various shapes.

Calculation of the elastic coefficients for a real rock media with complicated pore geometries is at present very difficult and is probably next to impossible. In this study, rather simple pore geometries are considered: the circular and rectangular pore shapes. It is assumed that these pores are distributed periodically in space in the solid rock medium. The pores are assumed to be saturated by water.

The theoretical framework is based on the homogenization theory which systematically combines the processes on the microscale(of order l) and deduces the governing equations and the effective coefficients on the macroscale(of order L) [1]. It is assumed that the two spatial scales are disparate so that $l \ll L$. Under two basic assumptions, (i) the periodicity of the medium structure on the microscale with periodic length l and (ii) the periodicity of all variables and material properties. The periodicity assumption is not very restrictive because the distributions and arrangements over the periodic length are quite arbitrary.

Starting from the basic governing laws on the microscale with multiple-scale perturbation expansion the governing laws on the macroscale are deduced with no recourse to empirical or experimental methods. During the process certain microscale boundary-value problems in a unit cell are defined whose solution is used in the calculation of the effective macroscale elastic coefficients. If the pore geometry is specified, the solution to the unit cell problem is found by numerical method which minimizes the variational principles that are obtained from the cell problem. Specifically, for the chosen pore geometries, the finite element method has been used to solve the unit cell problems

THE GOVERNING RELATIONS ON THE MICROSCALE

The porous medium is assumed to be composed of the matrix(Ωs) of solid rock phase and the fluid phase(Ω_f) that fills the pore space. Each phase is assumed to be connected throughout the porous medium. Fluid flow takes palce by macroscopically imposed pressure gradient over the medium.

The basic governing equations in the solid domain(Ωs) and the fluid domain(Ω_f) and the boundary conditions on the interface(Γ) are desribed.

In Ωs, the quasi-static equilibrium equation with Hooke's law must be satisfied.

In Ω_f, the basic governing equations on the microscale are the conservation of mass and the conservation of momentum[1].

On the boundary Γ between the solid and fluid, the continuity of the kinematic variables(the fluid velocity and the solid velocity), and the continuity of stress must be satisfied.

The governing equations and the boundary conditions are normalized by using the representative scales(refer to [1] for details.).

MULTIPLE SCALE ANALYSIS

The distinguishing features of the multiple scale perturbation analysis are briefly summarized. Recognizing the scale disparity in the process of elastic deformation, two distinct length scales are introduced: the microscale(the fast scale which is equivalent to the representative elementary volume in the traditional treatment of the process) and the macroscale(the scale over which the processes of interest take place from the viewpoint of reservoir engineering and management).

The variables are expanded as perturbation series in the following small parameter

$$\frac{\ell}{L} = \epsilon << 1 \qquad \text{(Eq. 1)}$$

in which ℓ is the microscale length and $L$is the macroscale length. Upon expansion of the governing equations and boundary conditions, the microscale boundary-value problems are investigated separately according to the respective order of ϵ and, through volume-averaging over the micro-cell, the effective macroscale governign equations are derived.

In the process of the multiple scale analysis, a few canonical micro-cell boundary-value problems are defined whose solutions are used in the calculation of the effective medium properties(effective macroscale coefficients) by averaging over the micro-cell volume.

THE MICRO-CELL BOUNDARY-VALUE PROBLEM

(1) If the solid displaement is expanded in a perturbation series,

$$\mathbf{v} = \mathbf{v}^{(0)} + \epsilon \mathbf{v}^{(1)} + \epsilon^2 \mathbf{v}^{(2)} + \cdots \qquad \text{(Eq. 2)}$$

The leading order term $\mathrm{v}^{(0)}$ is independent of the microscale and the correction term is expressed as

$$\mathbf{v}^{(1)} = \boldsymbol{\phi} : e'(\mathbf{v}^{(0)}) - \boldsymbol{\eta} p^{(0)} + < \mathbf{v}^{(1)} > = \phi_i^{mn} e'_{mn}(\mathbf{v}^{(0)}) - \eta_i p^{(0)} + < v_i^{(1)} > \qquad \text{(Eq. 3)}$$

where $p^{(0)}$ is the leading order fluid pressure, $< \mathrm{v}^{(1)} >$ is the unit cell average of $\mathrm{v}^{(1)}$, and the summation convention is assumed. From now on a pair of angle brackets denotes the unit cell average.

The third-order tensor $\boldsymbol{\phi} = \phi_i^{jk}$ and the vector $\boldsymbol{\eta} = \eta_i$ are solutions of the following problem:

$$\begin{array}{rcll}
\overline{\nabla} \cdot [\mathbf{a}^* : \bar{\mathrm{e}}(\boldsymbol{\phi})] + (\overline{\nabla} \cdot \mathbf{a}^*) : \mathbf{II} & = & 0 & \text{in} \quad \Omega_s \\
\overline{\nabla} \cdot [\mathbf{a}^* : \bar{\mathrm{e}}(\boldsymbol{\eta})] & = & 0 & \text{in} \quad \Omega_s \\
[\mathbf{a}^* : \bar{\mathrm{e}}(\boldsymbol{\phi})] \cdot \mathbf{N}^s & = & -(\mathbf{a}^* : \mathbf{II}) \cdot \mathbf{N}^s & \text{on} \quad \bar{\Gamma} \\
[\mathbf{a}^* : \bar{\mathrm{e}}(\boldsymbol{\eta})] \cdot \mathbf{N}^s & = & \mathbf{I} \cdot \mathbf{N}^s & \text{on} \quad \bar{\Gamma} \\
\boldsymbol{\phi} \ \text{ and } \ \boldsymbol{\eta} \ \text{ are} & & \Omega\text{-periodic.} & \\
\langle \boldsymbol{\phi} \rangle = \langle \boldsymbol{\eta} \rangle = 0 & & &
\end{array} \qquad \text{(Eq. 4)}$$

where a^* is the elastic coefficient of rank four and N^s is the outward normal vector on the interface pointing from the solid to fluid.

(2) After solving the elastostatic problems defined above the effective elastic coefficients and the pressure coefficients are calculated as[1]

$$\mathrm{a}' = \langle \mathrm{a}^* : [\mathbf{II} + \mathrm{e}(\boldsymbol{\phi})] \rangle \, ; \quad a'_{ijmn} = \left\langle a^*_{ijk\ell} : [\delta_{km}\delta_{\ell n} + e_{k\ell}(\boldsymbol{\phi}^{mn})\right\rangle \qquad \text{(Eq. 5)}$$

$$\boldsymbol{\alpha}' = n'\mathbf{I} \, \langle \mathrm{a}^* : \mathrm{e}(\boldsymbol{\eta}) \rangle : \quad \alpha'_{ij} = n'\delta_{ij} + \langle e_{ij}(\boldsymbol{\eta}) \rangle \qquad \text{(Eq. 6)}$$

VARIATIONAL PRINCIPLES FOR THE MICRO-CELL PROBLEMS

From the micro-cell elastostatic problems the following variational principles for $\boldsymbol{\phi}$ and $\boldsymbol{\eta}$ are derived(The derivation is omitted.)

$$\delta I = 0; \quad I = \frac{1}{2}\int_{\Omega_s} a^*_{ijk\ell} e_{ij}\left(\boldsymbol{\phi}^{mn}\right) e_{k\ell}\left(\boldsymbol{\phi}^{mn}\right) d\Omega + \int_{\bar{\Gamma}} a^*_{ijmn}\phi^{mn}_i N^s_j dA$$
$$\delta J = 0; \quad J = \frac{1}{2}\int_{\Omega_s} a^*_{ijk\ell} e_{ij}\left(\boldsymbol{\eta}\right) e_{k\ell}\left(\boldsymbol{\eta}\right) d\Omega - \int_{\bar{\Gamma}} \eta_i N^s_i dA \qquad \text{(Eq. 7)}$$

where the superscript symbol *mn* is for the elastic strain in the solid domain on the macroscale and no summation over *mn* is assumed. It is assumed that the solid phase is isotropic. Then

$$a^*_{ijk\ell} = \lambda^*\delta_{ij}\delta_{k\ell} + \mu^*\left(\delta_{ik}\delta_{j\ell} + \delta_{i\ell}\delta_{jk}\right), \qquad \lambda^* = \frac{\lambda}{E}, \quad \mu^* = \frac{\mu}{E} \qquad \text{(Eq. 8)}$$

in which λ^* and μ^* are dimensionless Lame’s constant and *E* is Young’s modulus.

COMPUTATIONAL DOMAIN

The pores(circular and square shapes) are located at the center of the micro-cell of square shape. The configuration of the cell is obvious and the sketch is not shown here. They will be shown later in the discussion of the numerical results. The radius of the circular pore and the half width of the square pore range from 0.1 to 0.4 of the cell size. Due to the symmetry of the pore geometry about the horizontal and vertical centerlines the computational domain is reduced to one quarter of the micro-cell. Hence the computation has been carried out in the reduced domain by using finite elements.

PROPERTIES OF THE SOLID ROCK MATERIAL

Typical elastic coefficients are summarized in Table 1 below in which ν.is Poisson’s ratio.

Table 1. Elastic coefficients of some rocks[2].

	$E(MPa)$	ν	λ^*	μ^*
Hackensack Siltstone	26,300	0.22	0.322	0.410
Flaming George shale	5,530	0.25	0.400	0.400
Micaceous shale	11,100	0.29	0.535	0.388
Cherokee marble	55,800	0.25	0.400	0.400
Nevada Test Site tuff	3,550	0.29	0.535	0.388

The following sets of values are chosen:

Material 1: λ^* = 0.4 and μ^* = 0.4

Material 2: λ^* = 0.8 and μ^* = 0.4

CONVERGENCE OF THE NUMERICAL SOLUTION

In order to check the accuracy of the numerical solution, several mesh discretizations have been used for a medium with Material 1 and a circular pore geometry with r_0 = 0.2(r_0 being the radius of the pore) and the results are summarized in Table 2 below.

Table 2. Convergence of displacements and the average stress for circular pore with r_0 = 0.2.

	Number of elements	$u(x = r_0, y = 0)$	$v(x = 0, y = r_0)$
Mesh 1	6	2.6411E-01	8.7144E-02
Mesh 2	24	2.7954E-01	9.6633E-02
Mesh 3	72	2.7963E-01	9.5750E-02
Mesh 4	192	2.7965E-01	9.5621E-02

	$< e_{xx} >$	$< e_{yy} >$	$< 2e_{xy} >$
Mesh 1	-1.6597E-01	-5.7868E-02	-2.8089E-01
Mesh 2	-1.7802E-01	-6.1220E-02	-2.8034E-01
Mesh 3	-1.7829E-01	-6.1110E-02	-2.7980E-01
Mesh 4	-1.7831E-01	-6.1102E-02	-2.7976E-01

The convergence pattern is more than satisfactory enough and 'Mesh 4' has been used throughout the computation.

NUMERICAL RESULTS AND DISCUSSION

Solid Displacement

The solid displacement caused by unit macroscale strain in *x*-direction only is shown.

(1) Circular pore

- For solid material type 1 (λ^* = 0.4 and μ^* = 0.4) the traction force acting on the interface is $\boldsymbol{t}$ = (1.2, 0) at $(x, y) = (r_0, 0)$ and $\boldsymbol{t}$ = (0,4. 0) at $(x, y) = (0, r_0)$ which is more than three times larger than that at $(x, y) = (r_0, 0)$. The displacement for various r_0 values is as shown in Fig. 1.

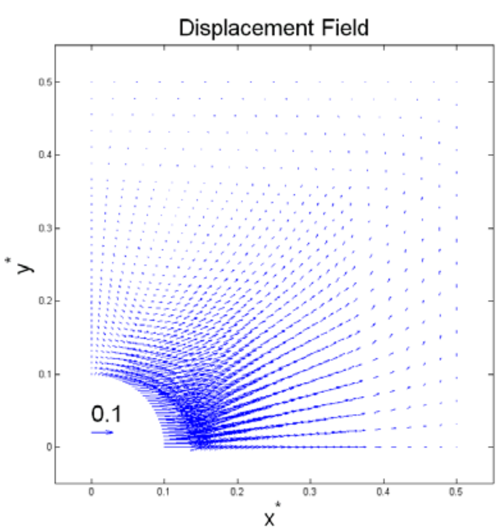

(a)

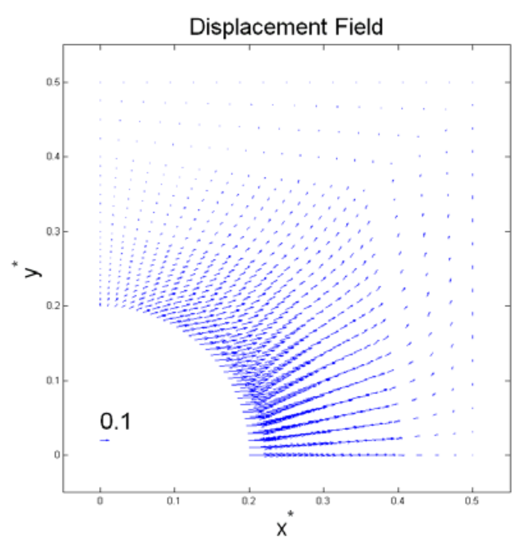

(b)

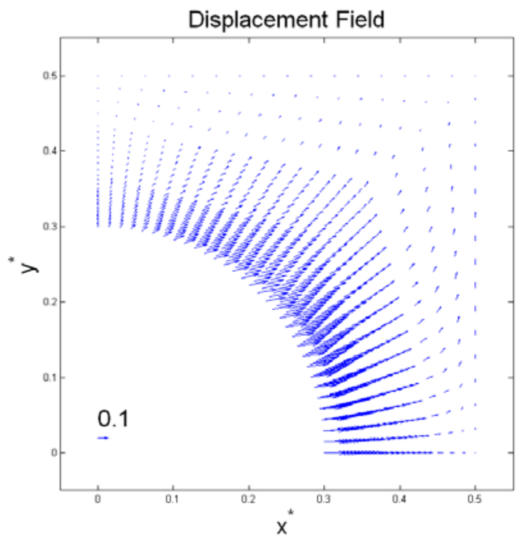

(c)

Fig. 1. Solid displacement in a unit cell made of Material 1 (λ^* = 0.4 and μ^* = 0.4) with a circular pore: (a) r_0 = 0.1, (b) r_0 = 0.2, and (c) r_0 = 0.3.

The contrast of the displacements at (x, y) = (r_0, 0) and (x, y) = (0, r_0) is the larger for smaller r_0, because the size of the solid domain to respond to the traction at the interface is larger for smaller r_0.

- For solid material type 2 (λ^* = 0.8 and μ^* = 0.4) the traction force acting the interface is ***t*** = (1.0, 0) at (x, y) = (r_0, 0) and ***t*** = (0, 0.2) at (x, y) = (0, r_0) which is ony one-fifth of the former. The displacement for various r_0 values is as shown in Fig. 2.

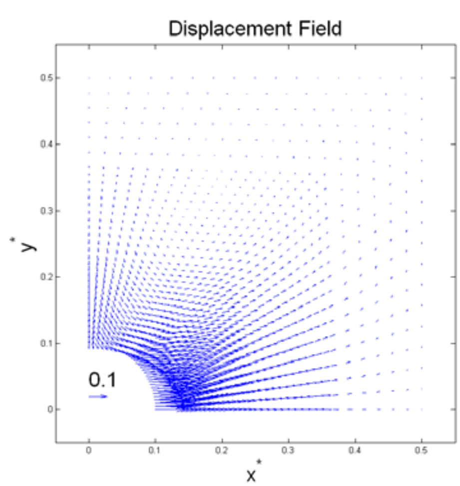

(a)

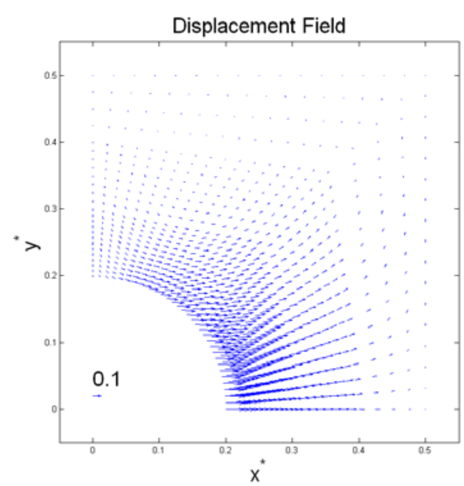

(b)

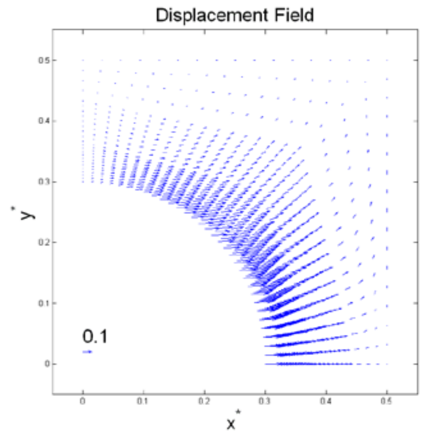

(c)

Fig. 2. Solid displacement in a unit cell made of Material 2 (λ^* = 0.8 and μ^* = 0.4) with a circular pore: (a) r_0 = 0.1, (b) r_0 = 0.2, and (c) r_0 = 0.3.

Although the contrast of the displacement at $(x, y) = (r_0, 0)$ and $(x, y) = (0, r_0)$ shows quite similar trend as in the case of Material 1, it is noted that the displacement at $(x, y) = (0, r_0)$ is pointing to the center even for compressive traction there, i.e., the movement of the interface is against the force acting on the interface.

(2) Square pore

- For solid material type 1 (λ^* = 0.4 and μ^* = 0.4) the traction force acting on the interface is $\boldsymbol{t}$ = (1.2, 0) at $(x, y) = (h/2, 0)$ and (0, 0.4) at $(x, y) = (0, h/2)$ where h is the width of the square pore. The displacement for various $h/2$ values is as shown in Fig. 3.

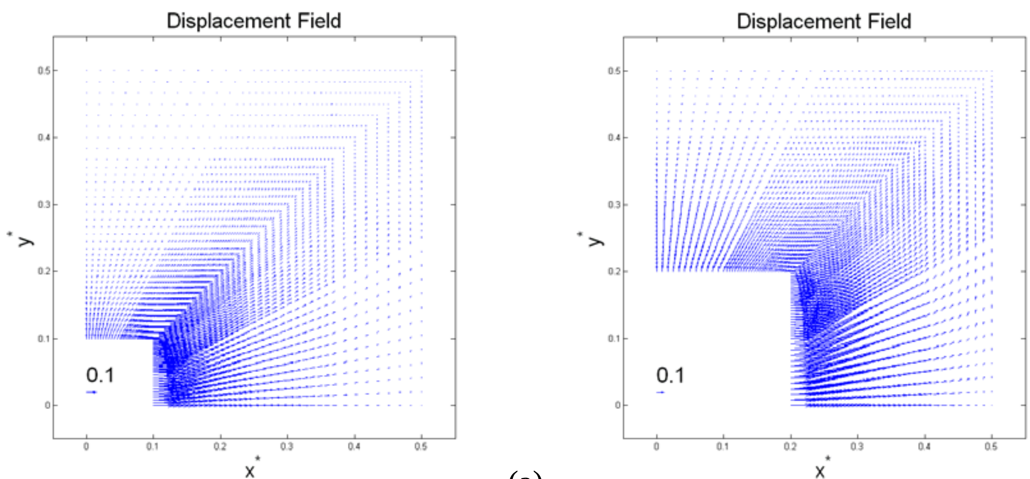

(a) (b)

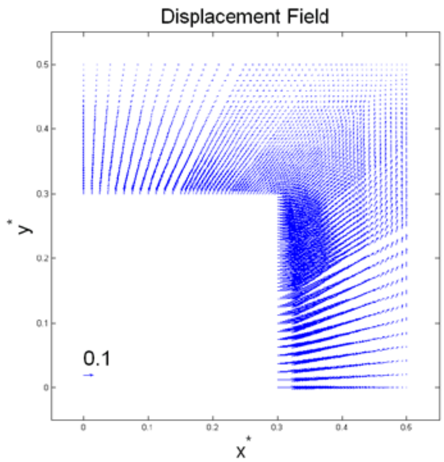

(c)

Fig. 3. Solid displacement in a unit cell made of Material 1 (λ^* = 0.4 and μ^* = 0.4) with a square pore: (a) $h/2$ = 0.1, (b) $h/2$ = 0.2, and (c) $h/2$ = 0.3.

As before the displacement is larger near (x, y) = (h/2, 0) and smaller near (x, y) = (0, h/2) due to different magnitudes of the traction forces. It should be noted that the displacement near the line y=x is the smallest because the solid region aroud that expands significantly as it gets farther from the origin.

- For solid material type 2 (λ^* = 0.8 and μ^* = 0.4) the traction force acting the interface is ***t*** = (1.0, 0) at (x, y) = (h/2, 0) and ***t*** = (0, 0.2) at (x, y) = (0, h/2) so that ***t*** at (x, y) = (h/2, 0) is five times larger than ***t*** at (x, y) = (0, h/2). The displacement for various h/2 values is as shown in Fig. 4.

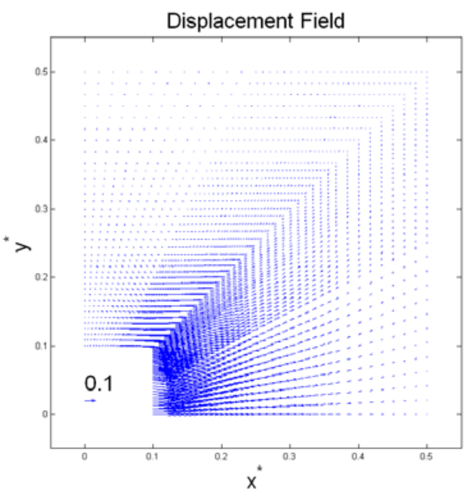

\- (a)

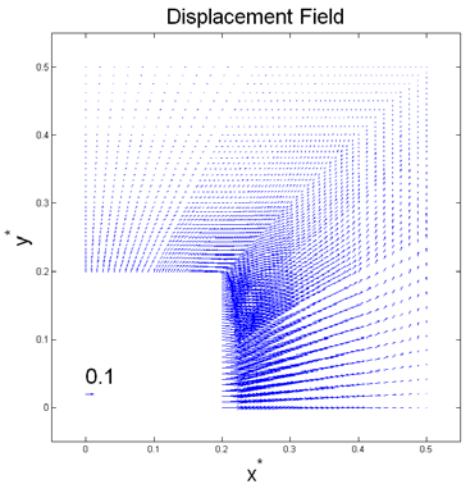

(b)

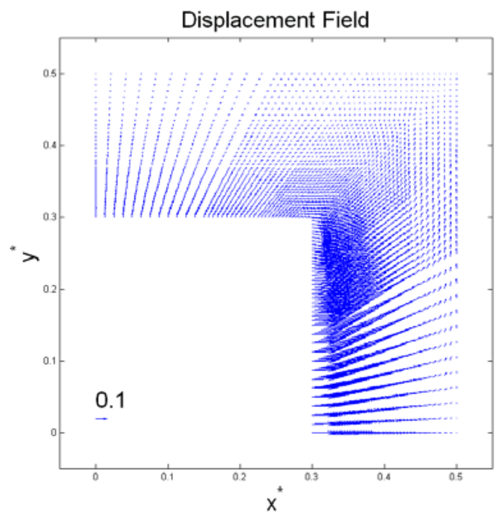

-

(c)

Fig. 4. Solid displacement in a unit cell made of Material 2 (λ^* = 0.8 and μ^* = 0.4) with a square pore: (a) $h/2$ = 0.1, (b) $h/2$ = 0.2, and (c) $h/2$ = 0.3.

The displacement pattern is to a certain extent similar to that for the case of circular pore in the sense that the interface in the region close to $(x, y) = (h/2, 0)$ shows larger displacement than that in the region close to $(x, y) = (0, h/2)$. The inward movement against the traction force near $(x, y) = (0, h/2)$ appears much weakened as compared to the case of circular pore due to flat shape of the interface.

Effective Macroscale Elastic Coefficients and Pressure Coefficients

The effective elastic coefficients in (5) specifically are written as

$$a'_{xxxx} = a'_{yyyy} = (1-n')a_I^* + \langle \sigma_{xx}(\boldsymbol{\phi}^{xx}) \rangle, \quad a'_{xxyy} = a'_{yyxx} = (1-n')a_{II}^* + \langle \sigma_{xx}(\boldsymbol{\phi}^{yy}) \rangle$$

$$a'_{xxzz} = a'_{zzxx} = (1-n')a_{II}^* + \langle \sigma_{xx}(\boldsymbol{\phi}^{zz}) \rangle, \quad a'_{zzzz} = (1-n')a_I^* + \langle \sigma_{zz}(\boldsymbol{\phi}^{zz}) \rangle \qquad \text{(Eq. 9)}$$

where n' is the porosity of the medium and the following are used:

$$a_I^* = a_{xxxx}^* = a_{yyyy}^* = a_{zzzz}^* \;,\quad a_{II}^* = a_{xxyy}^* \;,\quad \sigma_{ij}(\boldsymbol{\phi}^{mn}) = a_{ijk\ell}^* \left[e_{k\ell}(\boldsymbol{\phi}^{mn}) \right] \qquad \text{(Eq. 10)}$$

(1) Effective Elastic Coefficients

The coefficients a'_{ijmn} for a medium with Material 1 with circular and square pore geometries are shown in Fig. 5. First they decrease with r_0 or $h/2$ because the solid fraction decreases with increasing r_0 or $h/2$. Second, they appear to be slightly larger for a medium with circular pore than a medium with square pore because the solid fraction is a bit larger for a medium with circular pore. Third, a'_{zzzz} is larger than $a'_{xxxx} = a'_{yyyy}$ because along *z*-direction the geometry is preserved whereas along *x*- and *y*-directions the deformation of the pore geometry takes place rather easily. Fourth, a'_{xxyy} and a'_{xxzz} are very close to each other in both pore geometries. Last, $a'_{xxxx} = a'_{yyyy}$ is larger than a'_{xxyy} and a'_{xxzz} because the deformation in the transverse direction is induced more easily that the longitudinal direction.

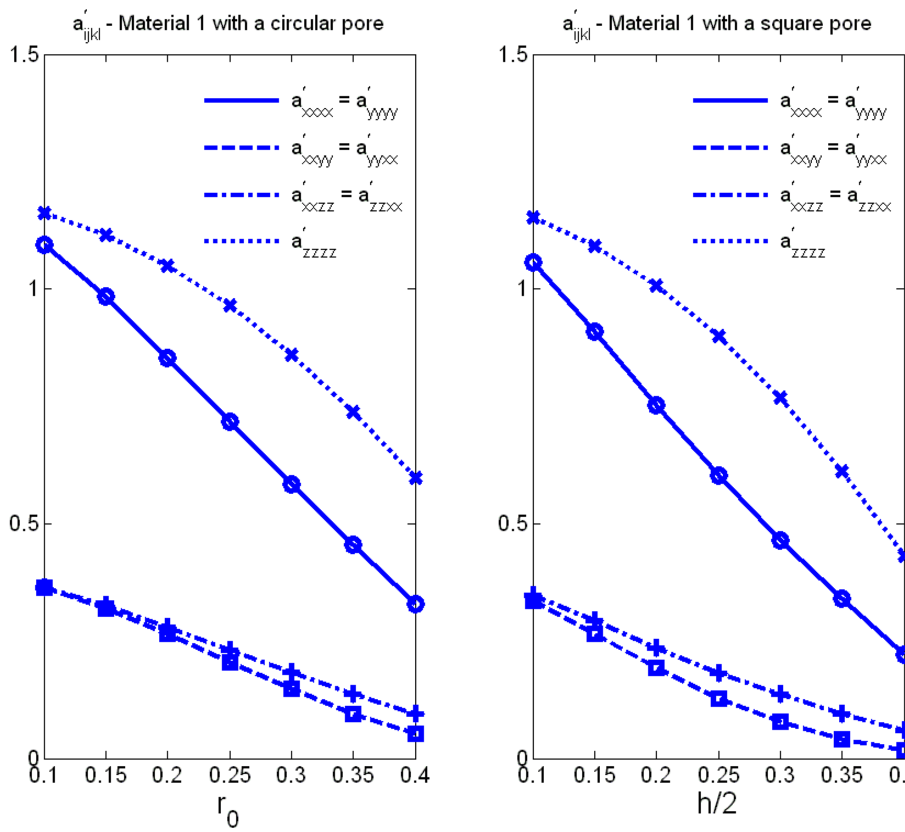

Fig. 5. The effective elastic coefficients for Material 1 with circular and square pores.

The coefficients a'_{ijmn} for a medium with Material 2 are shown in Fig. 6. The comments made for Material 1 are, in general, equally valid here. But, due to the difference in the Lame's constants, the values of a'_{ijmn} are higher for Material 2.

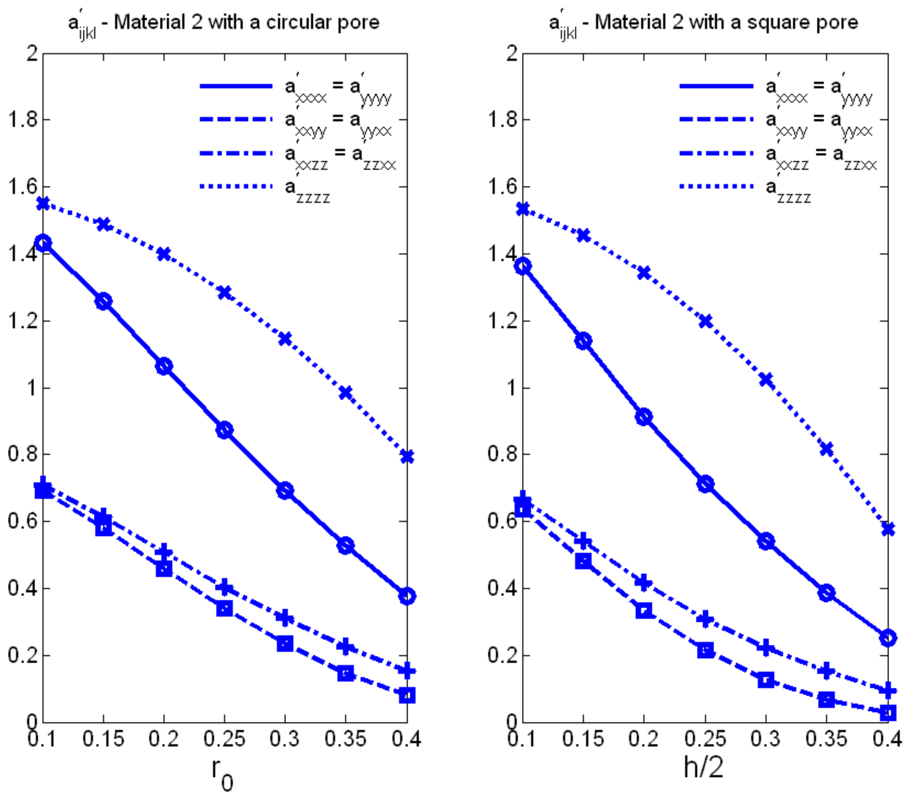

Fig. 6. The effective elastic coefficients for Material 2 with circular and square pores.

(2) Effective Pressure Coefficients

From (6) the effective pressure coefficients are

$$\alpha'_{xx} = n' + \langle \sigma_{xx}(\boldsymbol{\eta}) \rangle = \alpha'_{yy}\ , \quad \alpha'_{zz} = n' \quad \text{where} \quad \sigma_{ij}(\boldsymbol{\eta}) = a^*_{ijk\ell}\left[e_{k\ell}(\boldsymbol{\eta})\right] \qquad \text{(Eq. 11)}$$

The variation of α'_{xx} and α'_{zz} for Material 1 with r_0 and $h/2$ is shown in Fig. 7 and that for Material 2 is shown in Fig. 8. The values increase steadily with r_0 or $h/2$ because the fluid domain increases and hence the fluid pressure acting on the interface increases too. In the two-dimensional pore geometry considered here, the fluid pressure change cause by medium deformation in *xy*-plane is clearly very large in *x*- and *y*-directions whereas it is small in z-direction along which the pore channel is infinite. Hence α'_{xx} becomes larger than α'_{zz}. The pressure coefficients are larger for a medium with square pore that that with circular pore because, in the case of circular pore the compression effect on the interface is quickly spreading out in the solid domain due to the fanning effect into the solid.
The discrepancy of the pressure coefficients between Material 1 and Material 2 is such that the coefficients are larger for Material 2 as s result of the difference in the Lame's constants.

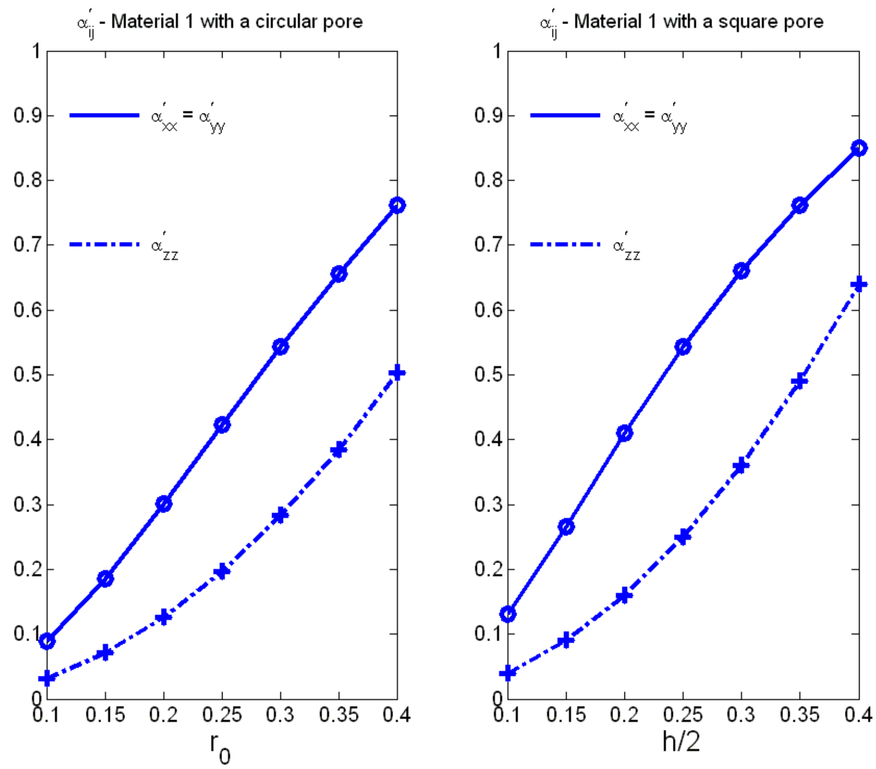

Fig. 7. The effective pressure coefficients for Material 1 with circular and square pores.

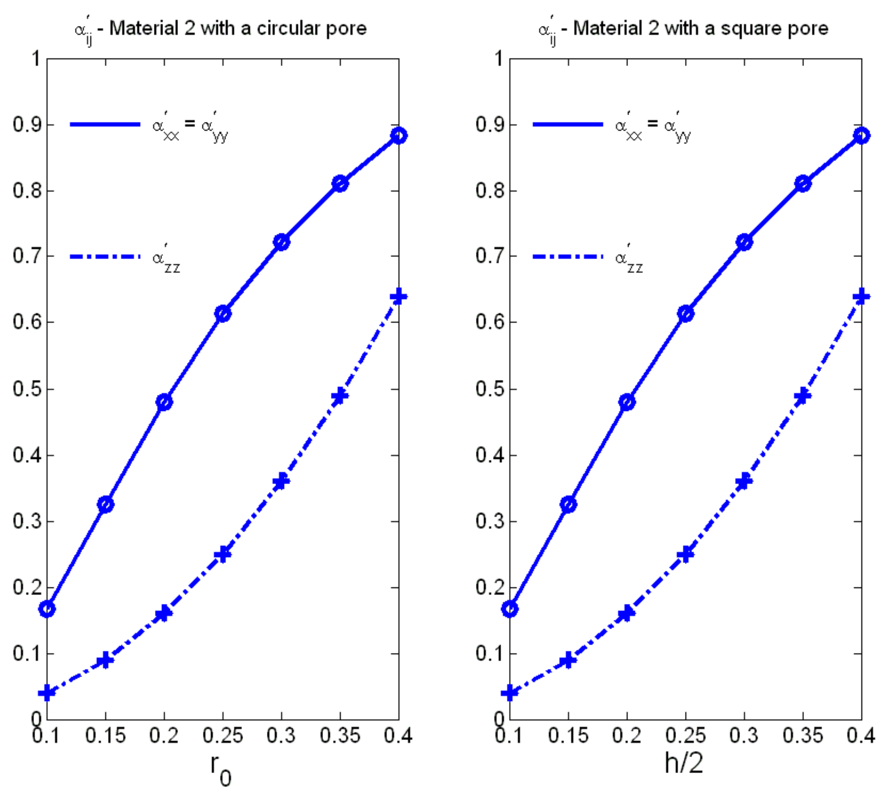

Fig. 8. The effective pressure coefficients for Material 2 with circular and square pores.

CONCLUSIONS

From the calculations of the solid displacements and the effective macroscale coefficients(the elastic coefficients and the pressure coefficients) for a porous medium with circular or square pore geometries the following conclusions are drawn.

1. The elastic coefficients decreases as the porosity increases due to the reduction of the solid domain that resists the traction force acting on the interface between the solid and fluid regions.

2. The elastic coefficient along the pore axis(a'_{zzzz}) is larger that those in the pore cross-section($a'_{xxxx} = a'_{yyyy}$) as a consequence of the geometrical characteristics.

3. The longitudinal elastic coefficient($a'_{xxxx} = a'_{yyyy}$) is larger than transverse ones(a'_{xxyy} and a'_{xxzz}).

4. The elastic coefficients are larger for a medium with larger λ^* which signifies the compressional strength of the solid region.

5. The pressure coefficients increase as the porosity increases due to increasing interface area on which the fluid pressure acts.

6. The pressure coefficient in the pore cross-section(α'_{xx}) is larger than that along the pore axis(α'_{zz}) due to increased resistance of the solid against the fluid pressure.

7. The pressure coefficients are larger for a medium with larger λ^*as in the case of the elastic coefficients.

ACKNOWLEDGEMENT

This research was supported by the National Research Foundation of Korea (Grant: NRF-2012R1A1A2041369) funded by the Ministry of Education, Science and Technology.

REFERENCE

1. Lee, C.K. (2004), “Flow and deformation in poroelastic media with moderate load and weak inertia. Proc. Roy. Soc. London A460, 2051-2087.
2. Goodman, R.E. (1989), Introduction to Rock Mechanics, 2nd ed., John Wiley & Sons.